

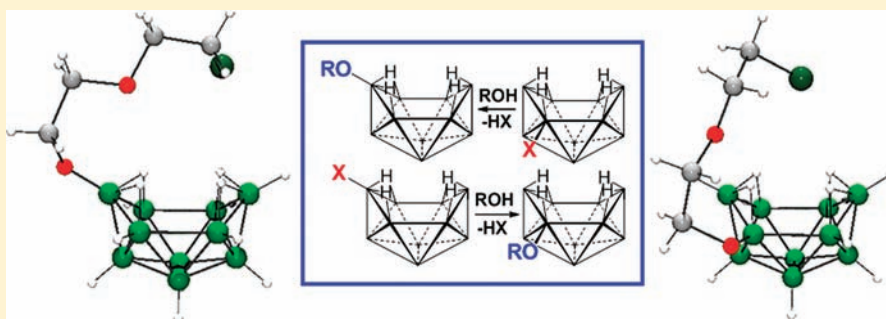
# Syntheses and Surprising Regioselectivity of 5- and 6-Substituted Decaboranyl Ethers via the Nucleophilic Attack of Alcohols on 6- and 5-Halodecaboranes

William C. Ewing, Patrick J. Carroll, and Larry G. Sneddon\*

Department of Chemistry, University of Pennsylvania Philadelphia, Pennsylvania 19104-6323, United States

Supporting Information

## ABSTRACT:



The selective syntheses of new classes of decaboranyl ethers containing a range of functional groups substituted at the B5 or B6 positions were achieved through the reaction of alcohols with halodecaboranes. The surprising regioselectivity of the reaction, where the reaction of the 6-halodecaboranes ( $6\text{-X-B}_{10}\text{H}_{13}$ ) with alcohols yielded the 5-substituted decaboranyl ethers ( $5\text{-RO-B}_{10}\text{H}_{13}$ ) and the reaction with 5-halodecaboranes ( $5\text{-X-B}_{10}\text{H}_{13}$ ) gave the 6-substituted decaboranyl ethers ( $6\text{-RO-B}_{10}\text{H}_{13}$ ), was confirmed by NMR and X-ray crystallographic analyses. The crystallographic determinations also showed that the decaboranyl ethers had shortened B–O bonds and apparent  $sp^2$  hybridization at oxygen indicating significant  $\pi$ -backbonding from oxygen to the cage boron. A possible substitution mechanism was computationally identified involving: (1) initial nucleophilic attack by the alcohol–oxygen at a site adjacent to the 5- or 6-halo-substituted boron, (2) movement of the terminal hydrogen at the point of attack to a bridging position, (3) formation of a 5-membered (B–O–H–Cl–B) cyclic transition state allowing the acidic methanolic–hydrogen to bond to the halogen, (4) release of HX, and finally (5) movement of a bridging hydrogen into the vacated terminal position. Deuterium labeling studies confirmed the movement of hydrogen from a bridging position of the halodecaborane into the halogen-vacated terminal position on the decaboranyl ether product. The relative reaction rates of the  $6\text{-X-B}_{10}\text{H}_{13}$  compounds ( $X = \text{F, Cl, Br, I}$ ) with alcohols were likewise found to be consistent with this mechanism.

## INTRODUCTION

We recently reported the selective, high yield syntheses of both the  $6\text{-X-B}_{10}\text{H}_{13}$  ( $X = \text{F, Cl, Br, I}$ )<sup>1</sup> and  $5\text{-X-B}_{10}\text{H}_{13}$  ( $X = \text{Cl, Br, I}$ )<sup>2</sup> series of halodecaboranes from *closo*- $\text{B}_{10}\text{H}_{10}^{2-}$  salts. These syntheses make these halo-derivatives readily available as potential new starting materials for the construction of functional decaboranyl derivatives for use in either biomedical or materials applications. We report here that the 5- or 6-halodecaboranes can be selectively converted, with a surprising regioselectivity, to new classes of  $6\text{-RO-B}_{10}\text{H}_{13}$  (**6OR**) and  $5\text{-RO-B}_{10}\text{H}_{13}$  (**5OR**) decaboranyl ethers via their nucleophilic substitution reactions with alcohols.

The B–O–C ether linkage has previously been found in only a few polyhedral boranes and carboranes. Examples include a number of *closo*- $\text{B}_{12}\text{H}_{(12-x)}(\text{OR})_x^{2-}$  and *closo*- $\text{B}_{10}\text{H}_{(10-x)}(\text{OR})_x^{2-}$  derivatives that were obtained by electrophilic substitution of terminal hydrides on the *closo*- $\text{B}_{12}\text{H}_{12}^{2-}$  and *closo*- $\text{B}_{10}\text{H}_{10}^{2-}$

anions<sup>3,4</sup> and the *p*-carborane ethers that were recently synthesized in good yields through the palladium mediated coupling of alkoxides and aryloxides with 2-iodo-*p*-carborane.<sup>5</sup> Several isomers of the metallaborane ether,  $\text{L}_2\text{PtB}_{10}\text{H}_{11}\text{OR}$  ( $R = \text{Et, Me, iPr}$ ), have also been synthesized in good overall yield through the cage-opening platination of *closo*- $\text{B}_{10}\text{H}_{10}^{2-}$  in alcoholic solutions.<sup>6</sup>

Only a few decaboranyl ethers have been reported. These have been obtained from the oxidation reactions of sodium decaborate ( $[\text{Na}^+][\text{B}_{10}\text{H}_{13}^-]$ ) using either  $\text{I}_2$  in organic ethers, which gave low yields (<26%) of  $\text{B}_{10}\text{H}_{13}\text{OR}$  products of unconfirmed regiochemistry,<sup>7</sup> or stannic chloride in diethyl ether, which produced a mix of 5- and 6- $\text{C}_2\text{H}_5\text{O-B}_{10}\text{H}_{13}$  (15:85; **5OR**:**6OR**) in unreported yields.<sup>8</sup> In contrast, the reactions presented in the following sections have now been shown to provide general

Received: December 22, 2010

Published: March 31, 2011

routes to a range of decaboranyl ethers with excellent control of regiochemistry.

## EXPERIMENTAL SECTION

**Materials.** The 5-X-B<sub>10</sub>H<sub>13</sub> (**5X**) and 6-X-B<sub>10</sub>H<sub>13</sub> (**6X**) (X = F, Cl, Br, I) compounds were synthesized according to literature procedures.<sup>12</sup> All alcohols, phenols, thiols, phenylthiols, deuterated alcohols (from Aldrich) and toluene, NaHCO<sub>3</sub>, CH<sub>2</sub>Cl<sub>2</sub>, hexanes, pentane, CDCl<sub>3</sub>, and D<sub>2</sub>O (from Fisher) were used as received. Silica gel (Fisher) was acidified according to the literature method prior to use.<sup>9</sup>

**Physical Methods.** <sup>11</sup>B NMR at 128.3 MHz and <sup>1</sup>H NMR at 400.1 MHz spectra were obtained on a Bruker DMX-400 spectrometer equipped with appropriate decoupling accessories. All <sup>11</sup>B chemical shifts were referenced to BF<sub>3</sub>·OEt<sub>2</sub> (0.0 ppm), with a negative sign indicating an upfield shift. All proton chemical shifts were measured relative to internal residual protons from the lock solvents (99.9% CDCl<sub>3</sub>) and then referenced to (CH<sub>3</sub>)<sub>4</sub>Si (0.0 ppm). High- and low-resolution mass spectra employing chemical ionization with negative ion detection were obtained on a Micromass AutoSpec high-resolution mass spectrometer. IR spectra were obtained on a Perkin-Elmer Spectrum 100 FT-IR spectrometer. Melting points were determined using a standard melting point apparatus and are uncorrected. Elemental analyses were obtained at Robertson Microlit Laboratories, Madison, NJ.

**General Reaction Methods.** Reactions were carried out in sealable 100 mL flasks, equipped with a stir bar, side arm, and Teflon stopcock (without a rubber O-ring), and were stirred after being sealed under N<sub>2</sub> at atmospheric pressure. Reactions were monitored by <sup>11</sup>B NMR; upon completion, the mixtures were diluted with hexanes and filtered, and the solvent was vacuum-evaporated. The products were isolated from the crude reaction mixture by initial flash filtration through a small plug of acidified silica gel, followed by either crystallization from cold pentanes or column-chromatography on acidified silica gel using a CH<sub>2</sub>Cl<sub>2</sub>/hexanes eluent. In cases where chromatography was employed, three materials were isolated: (1) residual starting material, (2) the desired isomer (5- or 6-RO-B<sub>10</sub>H<sub>13</sub>) as the major product, and (3) the other isomer as a minor product. The order of elution was always the starting material, then 6-RO-B<sub>10</sub>H<sub>13</sub>, and last 5-RO-B<sub>10</sub>H<sub>13</sub>. Isolated yields are given in Table 2. Detailed descriptions of the syntheses and spectroscopic data for the 6-(CH<sub>3</sub>O)- and 5-(CH<sub>3</sub>O)-decaboranyl ethers are presented below. Full experimental and spectroscopic details for all products are given in the Supporting Information.

**6-(CH<sub>3</sub>O)-B<sub>10</sub>H<sub>13</sub> (**6OMe**).** A mixture containing methanol (31 mg, 0.94 mmol), **5Br** (150 mg, 0.75 mmol), and NaHCO<sub>3</sub> (63 mg, 0.75 mmol) in 7 mL of CH<sub>2</sub>Cl<sub>2</sub> was stirred at 70 °C for 15 h. Additional methanol (15 mg, 0.26 mmol) was then added, and the reaction was stirred another 12 h at 65 °C. The reaction was diluted with 7 mL of hexanes and filtered. The filtrate solvent was vacuum evaporated at 0 °C to give a clear oil that was then taken up in a minimal amount of a 10% CH<sub>2</sub>Cl<sub>2</sub> in hexanes solution and chromatographed on acidic silica gel using the same eluent. For **6OMe**: 58 mg (0.38 mmol, 51%); clear oil; HRMS: *m/z* calcd for <sup>12</sup>C<sup>1</sup>H<sub>16</sub><sup>11</sup>B<sub>10</sub><sup>16</sup>O 154.2131, found 154.2152. <sup>11</sup>B NMR (128.3 MHz, *J* = Hz, CDCl<sub>3</sub>): δ 25.8 (s, 1B), 3.7 (d, *J* = ~125, 3B), 2.9 (d, *J* = ~125, 2B), -16.2 (d, *J* = 150, 2B), -32.6 (d, *J* = 158, 1B), -44.3 (d, *J* = 160, 1B). <sup>1</sup>H{<sup>11</sup>B} NMR (400.1 MHz, *J* = Hz, CDCl<sub>3</sub>): δ 3.91 (s, 1CH<sub>3</sub>, 1BH), 3.83 (s, 1BH), 3.23 (s, 4BH), 2.15 (s, 2BH), 1.42 (s, 1BH), 0.25 (s, 1BH), -0.52 (s, 2BHB), -1.81 (s, 2BHB). IR (KBr, cm<sup>-1</sup>) 3004 (w), 2951 (w), 2858 (w), 2579 (vs), 1556 (w), 1466 (s), 1327 (s), 1292 (s), 1265 (s), 1173 (w), 1114 (w), 1037 (w), 1004 (m), 994 (m), 959 (w), 927 (w), 913 (w), 881 (w), 841 (w), 805 (w), 734 (w), 718 (w), 703 (w), 684 (w), 639 (w), 578 (w).

**5-(CH<sub>3</sub>O)-B<sub>10</sub>H<sub>13</sub> (**5OMe**).** A mixture containing methanol (31 mg, 0.94 mmol), **6Br** (80 mg, 0.40 mmol), and NaHCO<sub>3</sub> (33 mg, 0.4 mmol) in 7 mL of CH<sub>2</sub>Cl<sub>2</sub> was stirred for 12 h at room temperature. The

mixture was diluted with 7 mL of hexanes and filtered. The filtrate was concentrated at 0 °C to give a yellowish oil that was then taken up in a minimal amount of a 50% CH<sub>2</sub>Cl<sub>2</sub> in hexanes solution and quickly filtered through a plug of acidic silica gel. The filtrate solvent was vacuum evaporated at 0 °C to give a clear oil that was then recrystallized from ~2 mL of pentane at -20 °C. For **5OMe**: 54 mg (0.36 mmol, 90%); white solid; mp 57–59 °C; Anal. Calcd.: C, 7.99%, H, 10.52%. Found: C, 7.17%, H, 11.14%; HRMS: *m/z* calcd for <sup>12</sup>C<sup>1</sup>H<sub>16</sub><sup>11</sup>B<sub>10</sub><sup>16</sup>O 154.2131, found 154.2312. <sup>11</sup>B NMR (128.3 MHz, *J* = Hz, CDCl<sub>3</sub>): δ 21.8 (s, 1B), 12.6 (d, *J* = 149, 1B), 10.5 (d, *J* = 162, 1B), 2.5 (d, *J* = ~115, 1B), 2.0 (d, *J* = ~150, 1B), -3.4 (d, *J* = 172, 1B), -6.5 (d, *J* = 161, 1B), -11.3 (d, *J* = 150, 1B), -38.9 (d, *J* = 155, 2B). <sup>1</sup>H{<sup>11</sup>B} NMR (400.1 MHz, *J* = Hz, CDCl<sub>3</sub>): δ 3.99 (s, 1BH), 3.76 (s, CH<sub>3</sub>), 3.66 (s, 1BH), 3.31 (s, 3BH), 2.76 (s, 1BH), 2.71 (s, 1BH), 0.99 (s, 1BH), 0.53 (s, 1BH), 0.34 (s, 1BHB), -1.98 (s, 1BHB), -2.22 (s, 1BHB), -2.38 (s, 1BHB). IR (KBr, cm<sup>-1</sup>) 2995 (m), 2944 (m), 2849 (m), 2579 (vs), 1894 (br,w), 1549 (w), 1461 (s), 1258 (vs), 1170 (s), 1104 (w), 1068 (w), 1047 (w), 1012 (s), 980 (m), 932 (w), 913 (w), 859 (w), 816 (m), 781 (m), 716 (m), 682 (w), 620 (w).

**Reactions of 6F, 6Cl, and 6I with CH<sub>3</sub>OH.** In three separate reactions, **6F**, **6Cl**, and **6I** (50 mg each, 0.36, 0.32, and 0.20 mmol, respectively) were reacted with methanol (1.3 equiv.) at room temperature while being monitored by <sup>11</sup>B NMR. The reaction with **6F** showed no change after 2 days. The reaction with **6Cl** was 25% complete after 2 days. The reaction with **6I** was complete after ~12 h.

**Reactions of 6Br with Phenol, 4-Methoxyphenol, Thiophenol, and 1-Octanethiol.** **6Br** (50 mg, 0.25 mmol) was separately reacted with phenol (28 mg, 0.30 mmol), 4-methoxyphenol (37 mg, 0.30 mmol), thiophenol (33 mg, 0.30 mmol), and 1-octanethiol (44 mg, 0.30 mmol) at both room temperature and at 70 °C in CH<sub>2</sub>Cl<sub>2</sub> for at least 20 h. No reaction, other than trace isomerization from **6Br** to **5Br**, was observed by <sup>11</sup>B NMR for any of the reactions at either temperature.

**Syntheses of μ-D<sub>4</sub>-5-Br-B<sub>10</sub>H<sub>9</sub> (μ-D<sub>4</sub>-5Br) and μ-D<sub>4</sub>-6-Br-B<sub>10</sub>H<sub>9</sub> (μ-D<sub>4</sub>-6Br).** In separate reactions, **5Br** (50 mg, 0.25 mmol) and **6Br** (50 mg, 0.25 mmol) were stirred in a biphasic mixture of 2 mL of CDCl<sub>3</sub> and 0.5 mL of D<sub>2</sub>O at room temperature. After 4 h, the <sup>1</sup>H{<sup>11</sup>B} NMR spectra of the CDCl<sub>3</sub> layers showed the disappearance of the high-field signals for all four bridging positions (Figures S1 and S2, Supporting Information). Neither <sup>11</sup>B NMR spectrum showed any change. The phases were separated, and the CDCl<sub>3</sub> layers containing the deuterated-decaborane products were then used without further workup in the subsequent experiments with CD<sub>3</sub>OD and CH<sub>3</sub>OH.

**Reaction of μ-D<sub>4</sub>-6Br with CD<sub>3</sub>OD and CH<sub>3</sub>OH.** In two separate experiments, CD<sub>3</sub>OD (~12 mg, 0.33 mmol) and CH<sub>3</sub>OH (~10 mg, 0.33 mmol) were added to a solution of ~50 mg of μ-D<sub>4</sub>-6Br in ~3 mL of CDCl<sub>3</sub> at room temperature. After the solution was stirred at room temperature for 10 h, <sup>11</sup>B NMR analysis indicated >90% conversion to μ-D<sub>3</sub>-6-D-5-(CD<sub>3</sub>O)-B<sub>10</sub>H<sub>9</sub> and μ-D<sub>3</sub>-6-D-5-(CH<sub>3</sub>O)-B<sub>10</sub>H<sub>9</sub>, respectively. The CDCl<sub>3</sub> was vacuum evaporated at 0 °C. The products were then purified by recrystallization from pentane at -78 °C.

**Reaction of 6Br with CD<sub>3</sub>OD.** CD<sub>3</sub>OD (~12 mg, 0.33 mmol) was added to a solution of ~50 mg of **6Br** in 2 mL of CDCl<sub>3</sub>. After the solution was stirred at room temperature for 10 h, <sup>11</sup>B NMR analysis indicated >90% conversion to 5-(CD<sub>3</sub>O)-B<sub>10</sub>H<sub>13</sub>. The CDCl<sub>3</sub> was vacuum evaporated at 0 °C. The product was then purified by recrystallization from pentane at -78 °C.

**Reaction of μ-D<sub>4</sub>-5Br with C<sub>2</sub>D<sub>5</sub>OD.** C<sub>2</sub>D<sub>5</sub>OD (~12 mg, 0.33 mmol) was added to a solution of ~50 mg of μ-D<sub>4</sub>-5Br in ~3 mL of CDCl<sub>3</sub>. After the solution was stirred at 70 °C for 10 h, <sup>11</sup>B NMR analysis indicated near quantitative conversion to μ-D<sub>3</sub>-5-D-6-(C<sub>2</sub>D<sub>5</sub>O)-B<sub>10</sub>H<sub>9</sub>. The CDCl<sub>3</sub> was vacuum evaporated at 0 °C to give an oil that was then taken up in a minimal amount of a 10% solution of CH<sub>2</sub>Cl<sub>2</sub> in hexanes and chromatographed on acidic silica gel using the same

eluent. The solvent from the fractions containing the  $\mu\text{-D}_3\text{-5-D-6-(C}_2\text{D}_5\text{O)-B}_{10}\text{H}_9$  product was vacuum evaporated at 0 °C.

**Computational Methods.** Density functional theory (DFT) calculations were performed using the Gaussian 03 package.<sup>10</sup> The optimized ground-state, transition-state, and intermediate geometries and both the electronic and free energy values were obtained at the B3LYP/6-311G(d) level without constraints for all H, C, B, and Cl atoms. Both the B3LYP/6-311G(d) level and B3LYP/SDD pseudopotential were used for Br atoms (separate calculations), but only the B3LYP/SDD pseudopotential was used for the I atoms. The NMR chemical shifts were calculated at the B3LYP/6-311G(d) level using the GIAO option within Gaussian 03 and are referenced to  $\text{BF}_3 \cdot \text{O}(\text{C}_2\text{H}_5)_2$  using an absolute shielding constant of 102.24 ppm. Harmonic vibrational analyses were carried out on the optimized geometries at the same level to establish the nature of stationary points. True first-order saddle points possessed only one imaginary frequency. Intrinsic reaction coordinate (IRC) calculations were carried out in both the forward and reverse directions to confirm the reaction pathways from the located transition states.

**Crystallographic Data.** All crystals were grown from cold pentane or by slow evaporation from heptane solution at –30 °C.

**Collection and Reduction of the Data.** Crystallographic data and structure refinement information are summarized in Table 1. X-ray intensity data for 6-( $\text{ClC}_2\text{H}_4\text{OC}_2\text{H}_4\text{O}$ )- $\text{B}_{10}\text{H}_{13}$  (Penn3371), 5-( $\text{ClC}_2\text{H}_4\text{OC}_2\text{H}_4\text{O}$ )- $\text{B}_{10}\text{H}_{13}$  (Penn3367), 5-( $\text{CH}_3\text{O}$ )- $\text{B}_{10}\text{H}_{13}$  (SOMe, Penn3364), and 5-( $\text{CH}_3\text{C}\equiv\text{CCH}_2\text{O}$ )- $\text{B}_{10}\text{H}_{13}$  (Penn3369) were collected on a Bruker APEXII CCD area detector employing graphite-monochromated Mo  $K\alpha$  radiation. Rotation frames were integrated using SAINT,<sup>11</sup> producing a list of unaveraged  $F^2$  and  $\sigma(F^2)$  values which were then passed to the SHELXTL<sup>12</sup> program package for further processing and structure solution on a Dell Pentium 4 computer. The intensity data were corrected for Lorentz and polarization effects and for absorption using SADABS.<sup>13</sup>

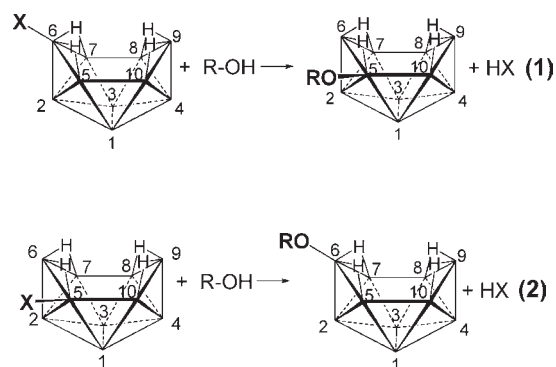
The data for 6-(( $\text{CH}_3$ )<sub>3</sub>CO)- $\text{B}_{10}\text{H}_{13}$  (Penn3349) and 6,6'-( $\text{OC}_6\text{H}_{10}\text{O}$ )-( $\text{B}_{10}\text{H}_{13}$ )<sub>2</sub> (Penn3351) were collected on a Rigaku Mercury CCD area detector employing graphite-monochromated Mo  $K\alpha$  radiation. Rotation frames were integrated using CrystalClear,<sup>14</sup> producing a list of unaveraged  $F^2$  and  $\sigma(F^2)$  values which were then passed to the CrystalStructure<sup>15</sup> program package for further processing and structure solution on a Dell Pentium 4 computer. The intensity data were corrected for Lorentz and polarization effects and for absorption using REQAB.<sup>16</sup>

**Solution and Refinement of the Structures.** The structures were solved by direct methods (SIR97<sup>17</sup>). Refinement was by full-matrix least-squares based on  $F^2$  using SHELXL-97.<sup>18</sup> All reflections were used during refinement (values of  $F^2$  that were experimentally negative were replaced with  $F^2 = 0$ ). For 6-( $\text{ClC}_2\text{H}_4\text{OC}_2\text{H}_4\text{O}$ )- $\text{B}_{10}\text{H}_{13}$ , 5-( $\text{ClC}_2\text{H}_4\text{OC}_2\text{H}_4\text{O}$ )- $\text{B}_{10}\text{H}_{13}$ , SOMe, 6-(( $\text{CH}_3$ )<sub>3</sub>CO)- $\text{B}_{10}\text{H}_{13}$ , and 6,6'-( $\text{OC}_6\text{H}_{10}\text{O}$ )-( $\text{B}_{10}\text{H}_{13}$ )<sub>2</sub>, all nonhydrogen atoms were refined anisotropically and hydrogen atoms were refined isotropically. For 5-( $\text{CH}_3\text{C}\equiv\text{CCH}_2\text{O}$ )- $\text{B}_{10}\text{H}_{13}$ , all nonhydrogen atoms were refined anisotropically and hydrogen atoms were refined isotropically, except for the methyl hydrogens which were refined using a riding model.

## RESULTS AND DISCUSSION

**Syntheses.** The only published account of the reaction of decaborane with alcohols reported degradation of the cage to  $\text{B}(\text{OR})_3$  compounds.<sup>19</sup> On the other hand, the reactions of the 5- and 6-halodecaboranes with alcohols led to the formation of decaboranyl ethers, with the loss of hydrogen halide. However, the observed regioselectivity was surprising, as the reactions with 6-X- $\text{B}_{10}\text{H}_{13}$  (6X) yielded 5-RO- $\text{B}_{10}\text{H}_{13}$  (SOR) products, while the reactions with 5-X- $\text{B}_{10}\text{H}_{13}$  (5X) produced the 6-RO- $\text{B}_{10}\text{H}_{13}$  (6OR) isomers (eqs 1 and 2). A variety of alcohols were employed as

nucleophiles, resulting in the production of a range of decaboranyl ether derivatives (Table 2).



The syntheses of the 5-RO- $\text{B}_{10}\text{H}_{13}$  derivatives were generally faster and required less purification than their 6-RO- $\text{B}_{10}\text{H}_{13}$  counterparts. Reactions with 6Br proceeded quickly at room temperature, while those with 5Br required heating (70 °C) to achieve completion. We have previously reported<sup>2</sup> that 5X and 6X undergo base-catalyzed isomerization to produce equilibrium mixtures of the two isomers favoring 5X. Since alcohols are only mildly basic, the rate of the base-catalyzed isomerizations of 5X and 6X in alcohols at room temperature was found to be slow compared to the halide substitution rate. Accordingly, the room temperature reactions of 6Br with alcohols afforded almost exclusively SOR products that could be easily purified. In contrast, the 5Br/6Br isomerization rate for the 5Br-alcohol reactions at 70 °C was found to be competitive with the 5Br substitution rate, with, for example, the <sup>11</sup>B NMR spectra of the reactions of 5Br with alcohols at 70 °C displaying small resonances for the 6Br isomer after ~1 h. As a consequence of the higher temperature required for the 5Br substitution reactions, a 6OR/SOR isomer mix was produced. Although 6OR was the major product, its isolation from this mixture required chromatographic separation in most cases.

Best yields were found when the products could be purified via crystallization. In agreement with a previous finding that decaboranyl ethers degrade on silica gel,<sup>8</sup> chromatographic separations resulted in decreased yields, especially when used to isolate SOR, as these compounds were both less stable and had longer retention times than the 6OR isomers. If the silica gel was not acidified<sup>9</sup> prior to use, complete SOR degradation was observed during chromatography. Both SOR and 6OR slowly degraded when left exposed to air for prolonged periods.

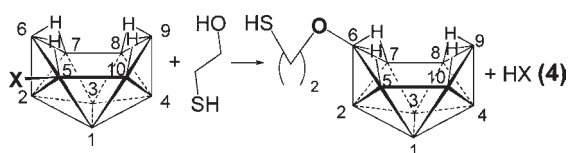
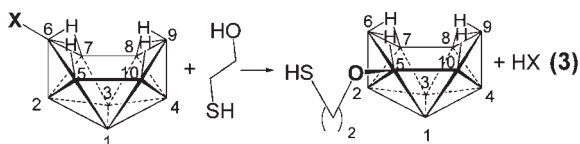
6Br showed no evidence of reaction with phenol at temperatures up to 90 °C, probably as a result of the decreased basicity (i.e., nucleophilicity) of the phenolic oxygen compared to alcohol oxygens. Even with the more strongly Lewis-basic *p*-methoxyphenol, no reaction was observed. The role of the relative basicity of the alcohol–oxygen was further examined through comparisons of the reaction rates of a series of  $\beta$ -halogenated alcohols with 6Br, where the relative halogen electronegativities were used to inductively alter the alcohol–oxygen electron density and Lewis basicity. In line with their predicted<sup>20</sup> Lewis basicities ( $\text{C}_2\text{H}_5\text{OH} > \text{IC}_2\text{H}_4\text{OH} > \text{BrC}_2\text{H}_4\text{OH} > \text{ClC}_2\text{H}_4\text{OH} > \text{FC}_2\text{H}_4\text{OH}$ ), the reaction of 6Br with ethanol was largely complete after 12 h at room temperature, but reactions with 2-iodoethanol (~20 h), 2-bromoethanol (~40 h), 2-chloroethanol (~100 h), and 2-fluoroethanol (~125 h) all took increasingly longer times.

Table 1. Crystallographic Data

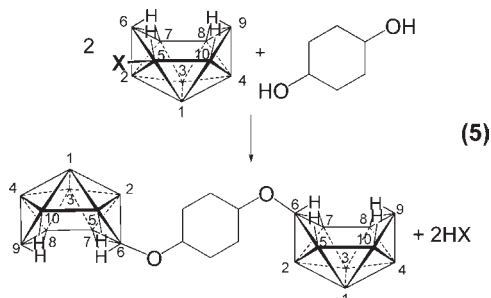
	6-(ClC <sub>2</sub> H <sub>4</sub> O-C <sub>2</sub> H <sub>4</sub> O)-B <sub>10</sub> H <sub>13</sub>	5-(ClC <sub>2</sub> H <sub>4</sub> O-C <sub>2</sub> H <sub>4</sub> O)-B <sub>10</sub> H <sub>13</sub>	5-(CH <sub>3</sub> O)-B <sub>10</sub> H <sub>13</sub>
empirical formula	C <sub>4</sub> B <sub>10</sub> H <sub>21</sub> O <sub>2</sub> Cl	C <sub>4</sub> B <sub>10</sub> H <sub>21</sub> O <sub>2</sub> Cl	CB <sub>10</sub> H <sub>16</sub> O
formula weight	244.76	244.76	152.24
crystal class	monoclinic	triclinic	monoclinic
space group	<i>P</i> 2 <sub>1</sub> / <i>n</i>	<i>P</i> $\bar{1}$	<i>P</i> 2 <sub>1</sub> / <i>c</i>
<i>Z</i>	4	2	4
<i>a</i> , Å	8.2214(10)	7.6495(15)	8.373(6)
<i>b</i> , Å	19.411(2)	9.7633(19)	9.848(9)
<i>c</i> , Å	9.2205(11)	11.127(3)	12.388(9)
$\alpha$ , deg		104.353(12)	
$\beta$ , deg	103.768(5)	106.187(13)	102.34(4)
$\gamma$ , deg		109.288(9)	
<i>V</i> , Å <sup>3</sup>	1429.2(3)	698.3(3)	997.9(14)
<i>D</i> <sub>calc</sub> g/cm <sup>3</sup>	1.138	1.164	1.013
$\mu$ , cm <sup>-1</sup>	2.43	2.49	0.48
$\lambda$ , Å (Mo-K $\alpha$ )	0.71073	0.71073	0.71073
crystal size, mm	0.28 × 0.25 × 0.08	0.35 × 0.30 × 0.08	0.44 × 0.35 × 0.08
<i>F</i> (000)	512	256	320
2 $\theta$ angle, deg	4.20–50.18	4.12–54.50	4.98–50.26
temperature, K	143(1)	143(1)	143(1)
<i>hkl</i> collected	−9 ≤ <i>h</i> ≤ 9 −23 ≤ <i>k</i> ≤ 23 −10 ≤ <i>l</i> ≤ 10	−9 ≤ <i>h</i> ≤ 8 −11 ≤ <i>k</i> ≤ 11 −13 ≤ <i>l</i> ≤ 13	−9 ≤ <i>h</i> ≤ 8 −8 ≤ <i>k</i> ≤ 11 −14 ≤ <i>l</i> ≤ 12
no. meas reflns	23645	12464	3795
no. of unique reflns	2533 ( <i>R</i> <sub>int</sub> = 0.0250)	2455 ( <i>R</i> <sub>int</sub> = 0.0222)	1736 ( <i>R</i> <sub>int</sub> = 0.0479)
no. parameters	239	239	174
<i>R</i> <sup>a</sup> indices ( <i>F</i> > 2 $\sigma$ )	<i>R</i> <sub>1</sub> = 0.0243 <i>wR</i> <sub>2</sub> = 0.0682	<i>R</i> <sub>1</sub> = 0.0346 <i>wR</i> <sub>2</sub> = 0.0889	<i>R</i> <sub>1</sub> = 0.0471 <i>wR</i> <sub>2</sub> = 0.1143
<i>R</i> <sup>a</sup> indices (all data)	<i>R</i> <sub>1</sub> = 0.0265 <i>wR</i> <sub>2</sub> = 0.0703	<i>R</i> <sub>1</sub> = 0.0383 <i>wR</i> <sub>2</sub> = 0.0928	<i>R</i> <sub>1</sub> = 0.0686 <i>wR</i> <sub>2</sub> = 0.1299
GOF <sup>b</sup>	1.058	1.041	0.974
final difference peaks, e/Å <sup>3</sup>	+0.166, −0.202	+0.444, −0.581	+0.206, −0.202
	6-((CH <sub>3</sub> ) <sub>3</sub> CO)-B <sub>10</sub> H <sub>13</sub>	5-(CH <sub>3</sub> C≡CCH <sub>2</sub> O)-B <sub>10</sub> H <sub>13</sub>	6,6'-(OC <sub>6</sub> H <sub>10</sub> O)-(B <sub>10</sub> H <sub>13</sub> ) <sub>2</sub>
empirical formula	C <sub>4</sub> B <sub>10</sub> H <sub>22</sub> O	C <sub>4</sub> B <sub>10</sub> H <sub>18</sub> O	C <sub>6</sub> B <sub>20</sub> H <sub>36</sub> O <sub>2</sub>
formula weight	194.32	190.28	356.55
crystal class	monoclinic	triclinic	monoclinic
space group	<i>P</i> 2 <sub>1</sub>	<i>P</i> $\bar{1}$	<i>P</i> 2 <sub>1</sub> / <i>c</i>
<i>Z</i>	2	4	2
<i>a</i> , Å	5.8342(4)	7.094(3)	16.600(2)
<i>b</i> , Å	10.4766(7)	12.518(5)	6.6881(9)
<i>c</i> , Å	10.5591(7)	14.907(6)	10.1106(14)
$\alpha$ , deg		68.796(15)	
$\beta$ , deg	96.879(2)	86.318(18)	91.691(3)
$\gamma$ , deg		77.129(15)	
<i>V</i> , Å <sup>3</sup>	640.75(7)	1202.9(9)	1122.0(3)
<i>D</i> <sub>calc</sub> g/cm <sup>3</sup>	1.007	1.051	1.055
$\mu$ , cm <sup>-1</sup>	0.49	0.52	0.51
$\lambda$ , Å (Mo-K $\alpha$ )	0.71073	0.71073	0.71073
crystal size, mm	0.30 × 0.22 × 0.08	0.42 × 0.25 × 0.15	0.38 × 0.32 × 0.03
<i>F</i> (000)	208	400	376
2 $\theta$ angle, deg	5.25–50.08	3.72–50.26	6.56–50.00
temperature, K	143(1)	143(1)	143(1)
<i>hkl</i> collected	0 ≤ <i>h</i> ≤ 6 0 ≤ <i>k</i> ≤ 12 −12 ≤ <i>l</i> ≤ 12	−8 ≤ <i>h</i> ≤ 8 −14 ≤ <i>k</i> ≤ 14 −17 ≤ <i>l</i> ≤ 17	−19 ≤ <i>h</i> ≤ 19 −7 ≤ <i>k</i> ≤ 7 −11 ≤ <i>l</i> ≤ 12
no. meas reflns	10744	30153	11522
no. of unique reflns	2374 ( <i>R</i> <sub>int</sub> = 0.0242)	4260 ( <i>R</i> <sub>int</sub> = 0.0215)	1968 ( <i>R</i> <sub>int</sub> = 0.0340)
no. parameters	226	394	200
<i>R</i> <sup>a</sup> indices ( <i>F</i> > 2 $\sigma$ )	<i>R</i> <sub>1</sub> = 0.0346 <i>wR</i> <sub>2</sub> = 0.0929	<i>R</i> <sub>1</sub> = 0.0416 <i>wR</i> <sub>2</sub> = 0.1176	<i>R</i> <sub>1</sub> = 0.0462 <i>wR</i> <sub>2</sub> = 0.1063
<i>R</i> <sup>a</sup> indices (all data)	<i>R</i> <sub>1</sub> = 0.0361 <i>wR</i> <sub>2</sub> = 0.0937	<i>R</i> <sub>1</sub> = 0.0464 <i>wR</i> <sub>2</sub> = 0.1210	<i>R</i> <sub>1</sub> = 0.0580 <i>wR</i> <sub>2</sub> = 0.1141
GOF <sup>b</sup>	1.113	1.042	1.053
final difference peaks, e/Å <sup>3</sup>	+0.115, −0.145	+0.294, −0.252	+0.161, −0.168

<sup>a</sup> $R_1 = \sum ||F_o| - |F_c|| / \sum |F_o|$ ;  $wR_2 = \{\sum w(F_o^2 - F_c^2)^2 / \sum w(F_o^2)^2\}^{1/2}$ . <sup>b</sup>GOF =  $\{\sum w(F_o^2 - F_c^2)^2 / (n - p)\}^{1/2}$  where *n* = no. of reflns; *p* = no. of params refined.

Mercapto-compounds also failed to react, despite their enhanced Lewis basicity relative to phenols. This result may be thermodynamically explained, as a nondative B–S bond (85–90 kcal/mol)<sup>21</sup> is weaker than a similar B–O bond (117–119 kcal/mol)<sup>22</sup> and DFT calculations showed that the reaction of methanol with **6Br** to yield **5OMe** was –10.0 kcal/mol downhill, while the reaction employing methylthiol was +5.6 kcal/mol uphill. This selectivity for oxygen allowed the synthesis of the 6- and 5-(HSC<sub>2</sub>H<sub>4</sub>O)-B<sub>10</sub>H<sub>13</sub> thiol-derivatives through the reaction of **5Br** or **6Br** with 2-mercaptoethanol (eqs 3 and 4).



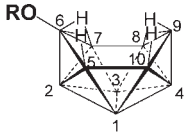
The reaction of 1,4-cyclohexyldiol with both **5Br** and **6Br** yielded the compounds 6,6'-(OC<sub>6</sub>H<sub>10</sub>O)-(B<sub>10</sub>H<sub>13</sub>)<sub>2</sub> (eq 5) and 5,5'-(OC<sub>6</sub>H<sub>10</sub>O)-(B<sub>10</sub>H<sub>13</sub>)<sub>2</sub>, respectively, each bridged by a diol.



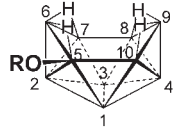
The potential tumor binding properties of thiol-derivatives,<sup>23</sup> such as 6- and 5-(HSC<sub>2</sub>H<sub>4</sub>O)-B<sub>10</sub>H<sub>13</sub>, and the high-boron contents of polyol derivatives, such as 6,6'-(OC<sub>6</sub>H<sub>10</sub>O)-(B<sub>10</sub>H<sub>13</sub>)<sub>2</sub> and 5,5'-(OC<sub>6</sub>H<sub>10</sub>O)-(B<sub>10</sub>H<sub>13</sub>)<sub>2</sub>, may prove useful in the design of new therapeutic agents for boron neutron capture therapy (BNCT) where high boron content compounds that selectively bind tumor cells are required.<sup>24</sup>

**NMR and Crystallographic Characterizations of 6OR and 5OR.** Regardless of the identity of the ether substituents, the <sup>11</sup>B NMR spectra of the **5OR** compounds were similar, as were the spectra of the **6OR** ethers. The <sup>11</sup>B NMR spectra of the **5OR** compounds, as illustrated in Figure 1a,b for 5-(C<sub>6</sub>H<sub>11</sub>O)-B<sub>10</sub>H<sub>13</sub>, **5OCy**, displayed 9 peaks (B2 and B4 are coincident at ~40 ppm) consistent with the predicted C<sub>1</sub> symmetry, with the low-field singlet arising from the ether-substituted B5 vertex. When the cages were substituted with primary alcohols, the separation between the 2 resonances between 0.0 and +5.0 ppm (B1 and B10, respectively) decreased; in some cases, these peaks were coincident, but the shifts of the other resonances were nearly identical regardless of the alcohol employed. The <sup>11</sup>B NMR spectra of the **6OR** compounds showed only 5 resonances in 1:5:2:1:1 ratios, as can be seen in the spectra of 6-(C<sub>6</sub>H<sub>11</sub>O)-B<sub>10</sub>H<sub>13</sub> (**6OCy**)

**Table 2.** Isolated Yields for 6-RO-B<sub>10</sub>H<sub>13</sub> and 5-RO-B<sub>10</sub>H<sub>13</sub>



-OR	% yield
-OCH <sub>3</sub>	51
-OC <sub>6</sub> H <sub>11</sub>	48
-OC(CH <sub>3</sub> ) <sub>3</sub>	42
-O(CH <sub>2</sub> ) <sub>3</sub> C≡CH	66
-OCH(CH <sub>2</sub> CH=CH <sub>2</sub> ) <sub>2</sub>	62
-OC <sub>2</sub> H <sub>4</sub> SH	49
-OC <sub>4</sub> H <sub>2</sub> I	45
-OC <sub>2</sub> H <sub>4</sub> OC <sub>2</sub> H <sub>4</sub> Cl	62
-OC <sub>6</sub> H <sub>10</sub> O-	25



-OR	% yield
-OCH <sub>3</sub>	90
-OC <sub>6</sub> H <sub>11</sub>	77
-OC(CH <sub>3</sub> ) <sub>3</sub>	75
-O(CH <sub>2</sub> ) <sub>3</sub> C≡CH	38
-O(CH <sub>2</sub> C≡CCH <sub>3</sub> )	72
-OCH(CH <sub>2</sub> CH=CH <sub>2</sub> ) <sub>2</sub>	48
-OC <sub>2</sub> H <sub>4</sub> SH	88
-OC <sub>4</sub> H <sub>2</sub> I	69
-OC <sub>2</sub> H <sub>4</sub> (NC <sub>4</sub> H <sub>4</sub> O <sub>2</sub> )	74
-OC <sub>2</sub> H <sub>4</sub> OC <sub>2</sub> H <sub>4</sub> Cl	80
-OC <sub>6</sub> H <sub>10</sub> O-	19

in Figure 1c,d, in line with the C<sub>s</sub> symmetry of this isomer. Again, the resonance for the ether-substituted vertex (B6) was found at the lowest field.

Table 3 compares the experimentally observed and DFT/GIAO-calculated <sup>11</sup>B NMR chemical shifts and assignments for both the **6OCy** and **5OCy** isomers. In contrast to the calculated shifts for the 5- and 6-halodecaboranes, which showed excellent agreement with the observed experimental values,<sup>1,2</sup> a number of the calculated decaboranyl ether shifts showed somewhat larger than normal differences (>4 ppm) between the computational and experimentally observed shifts. The calculated shifts for the ether-substituted B6 vertex of **6OCy** and its immediate neighbor borons (B2, B5, and B7) had the poorest agreement. Nevertheless, the assignments of all of the **5OCy** and **6OCy** resonances were confirmed through the combined use of the DFT calculations and 2D COSY <sup>11</sup>B–<sup>11</sup>B

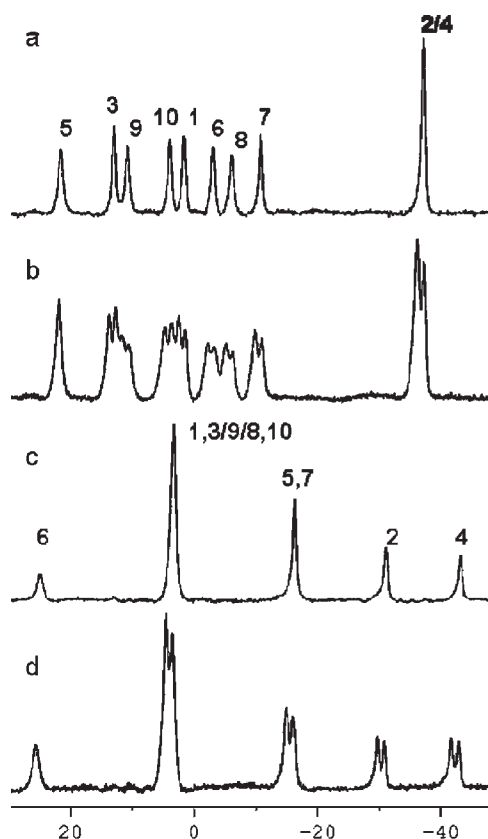


**Figure 1.** (a)  $^{11}\text{B}\{^1\text{H}\}$  NMR spectrum of **5OCy**; (b)  $^{11}\text{B}$  NMR spectrum ( $^1\text{H}$ -coupled) of **5OCy**; (c)  $^{11}\text{B}\{^1\text{H}\}$  NMR spectrum of **6OCy**; (d)  $^{11}\text{B}\{^1\text{H}\}$  NMR spectrum of **6OCy**. The spectra are typical of all compounds synthesized with similar regiochemistry. Peaks are labeled with their vertex assignment. For the numbering scheme, see Table 2.

**Table 3.** DFT/GIAO (B3LYP/6-311G(d)) Calculated and Observed  $^{11}\text{B}$  NMR Shifts (ppm) of **6OCy** and **5OCy**<sup>a</sup>

	calc.	assign.		calc.	assign.
B1,3	6.2	3.4	B1	3.1	0.9
B2	-38.1	-31.9	B2	-41.5	-38.3
B4	-46.0	-44.2	B3	16.6	12.6
B5,7	-11.6	-16.6	B4	-41.6	-38.3
B6	19.5	25.5	B5	22.2	21.3
B8,10	1.7	3.4	B6	-9.2	-3.9
B9	3.6	3.4	B7	-13.6	-11.8
			B8	-6.1	-6.9
			B9	6.6	10.3
			B10	5.5	3.3

<sup>a</sup> Assignments are consistent with DFT calculated values and 2D COSY  $^{11}\text{B}$ - $^{11}\text{B}$  NMR in Figures S3 and S4, Supporting Information.

NMR experiments (Figures S3 and S4, Supporting Information) carried out on **6OMe** and **5OMe**.

As shown in the spectrum of  $6\text{-}((\text{CH}_2=\text{CHCH}_2)_2\text{HCO})\text{-B}_{10}\text{H}_{13}$  (Figure S5, Supporting Information), the  $^1\text{H}$  NMR spectra of the **6OR** compounds showed, in addition to the C-H resonances, two intensity-2 bridging-hydrogen resonances, along with 5 terminal B-H resonances in 1:4:2:1:1 ratios in line with their  $C_s$ -symmetric structures. The  $^1\text{H}$  NMR spectra of the **5OR** isomers, as shown in the spectrum of  $5\text{-}((\text{CH}_2=\text{CHCH}_2)_2\text{HCO})\text{-B}_{10}\text{H}_{13}$  (Figure S6, Supporting Information), had similar C-H resonances, but in agreement with their  $C_1$ -symmetric structures, exhibited seven terminal B-H resonances in 1:1:3:1:1:1:1 ratios along with four intensity-1 bridging-proton resonances. As was previously observed in the  $^1\text{H}$  NMR spectra of the **5X** compounds,<sup>2</sup> three of the bridge protons were positioned upfield (above  $-1.5$  ppm), while the other was at lower field near 0.5 ppm. A 2D HCOR  $^{11}\text{B}$ - $^1\text{H}$  NMR experiment (Figure S7, Supporting Information) confirmed that the lower-field bridge resonance arises from the proton at the B5-B6 edge that is adjacent to the B5-ether substituent.

ORTEP drawings of the crystallographically determined structures are shown in Figures 2, 3, 4, 5, and 6. Comparisons of the B-B intracage bond distances in both the 5- and 6-substituted decaboranyl ethers with the **5X** and **6X** halodecaboranes, respectively,<sup>1,2</sup> showed no significant differences. Likewise, as was the case for the halodecaboranes,<sup>1,2</sup> there were no significant differences in the intracage B-B bond lengths in the **5OR** and **6OR** isomers.

Significant backbonding interactions from  $\pi$ -donating substituents on polyborane cages have been previously observed in both halogenated and amino-substituted derivatives.<sup>1,2,25</sup> Backbonding from O to B in the decaboranyl ethers was evidenced by shortened B-O bonds and an  $sp^2$  hybridized oxygen. Table 4 compares the values for the B-O bonds lengths and the B-O-C angles in the decaboranyl ethers with those found in  $\text{B}(\text{OCH}_3)_3$ ,<sup>26</sup> where  $\pi$ -backbonding is strong, and in  $\text{B}(\text{OCH}_3)_4^-$ ,<sup>27</sup> where  $\pi$ -backbonding is impossible. The B-O bond lengths in the 5- and 6-decaboranyl ethers (ranging from  $\sim 1.33$  Å to  $\sim 1.37$  Å) are quite similar to those found in  $\text{B}(\text{OMe})_3$  (1.359(6) Å) and significantly shorter than those in  $\text{B}(\text{OCH}_3)_4^-$  ( $\sim 1.46$  Å, average). The decaboranyl ether B-O-C bond angles were all near  $120^\circ$ , consistent with an  $sp^2$  hybridization of the cage-bound oxygen that would optimize  $\pi$ -backbonding. The B-O-C angle in  $\text{B}(\text{OCH}_3)_3$  is similar, at  $119.7^\circ$ , while the same angle in  $\text{B}(\text{OCH}_3)_4^-$  is only  $116^\circ$ .

As can also be seen in Table 4, the B-O bond lengths and B-O-C angles in the decaboranyl ether compounds are more similar to that found in  $2\text{-}(\text{CH}_3\text{O})\text{-1,12-C}_2\text{B}_{10}\text{H}_{11}$  (1.3884(16) Å and  $119.76(10)^\circ$ )<sup>5</sup> than to those of the anionic  $(\text{C}_2\text{H}_5\text{O})\text{-B}_{12}\text{H}_{11}^{2-}$  (1.442(5) Å and  $115.9(3)^\circ$ )<sup>28</sup> and  $2\text{-}(\text{ClC}_4\text{H}_8\text{O})\text{-1-CB}_{11}\text{H}_{11}^-$  (1.409(3) Å and  $118.4(2)^\circ$ )<sup>29</sup> clusters consistent with the greater degree of O to B backbonding that would be expected for the neutral polyborane ethers.

**Computational Studies of the Reaction Pathway.** As described earlier, the substitution reactions in eqs 1 and 2 proceeded with surprising regioselectivities. Nevertheless, it was possible to identify reasonable pathways for the transformations of **6X** to **SOME** and **5X** to **6OMe** using DFT/IRC calculations. As can be seen in Figure 7 for the reaction of **6Cl** with methanol, nucleophilic attack of the alcohol-oxygen at B5 pushes its terminal hydrogen upward to form the **TS1** transition state. In **TS1**, the oxygen is still 2.23 Å from B5 and the B-Cl bond has

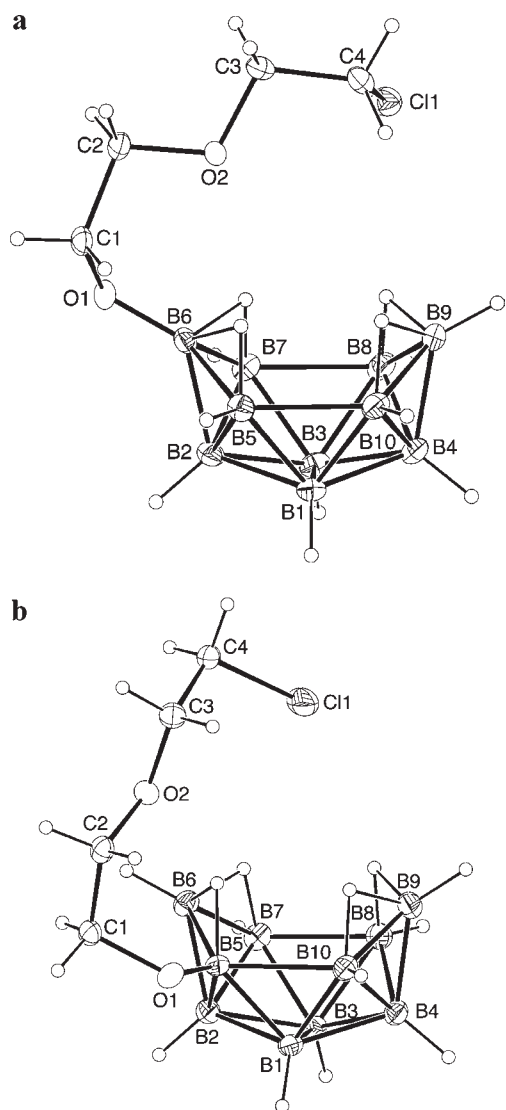


**Figure 2.** ORTEP drawings of the crystallographically determined structures of (a) 6-(ClC<sub>2</sub>H<sub>4</sub>OC<sub>2</sub>H<sub>4</sub>O)-B<sub>10</sub>H<sub>13</sub>, (b) 5-(ClC<sub>2</sub>H<sub>4</sub>OC<sub>2</sub>H<sub>4</sub>O)-B<sub>10</sub>H<sub>13</sub>. Selected bond distances (Å) and angles (°) for: (a) B6–O1, 1.3548(13); O1–C1, 1.4364(13); B6–B5, 1.8025(17); B5–B10, 1.9631(18); B5–B2, 1.8021(17); B6–B2, 1.7327(16); B9–B10, 1.7924(19); B9–B4, 1.7180(17); C1–O1–B6, 120.74(8); O1–B6–B5, 129.07(9); B6–B5–B10, 117.65(8); O1–B6–B2, 131.82(9); B5–B6–B7, 104.63(8); B8–B9–B10, 104.60(8). (b) B5–O1, 1.3604(19); O1–C1, 1.4372(17); B5–B6, 1.810(2); B5–B10, 2.031(2); B8–B7, 1.939(2); B6–B7, 1.798(2); B5–B2, 1.826(2); B5–B1, 1.770(2); B6–B2, 1.733(2); B4–B9, 1.723(2); B2–B7, 1.775(2); C1–O1–B5, 122.93(11); B6–B5–B10, 115.19(11); O1–B5–B2, 132.56(13); O1–B5–B1, 121.13(12); B5–B10–B9, 115.75(11); B5–B1–B10, 70.73(10); O1–B5–B10, 111.63(11); O1–B5–B6, 125.81(12); B5–B6–B7, 105.36(11); B8–B9–B10, 105.18(12).

only slightly lengthened from 1.78 to 1.82 Å. As the oxygen moves closer to B5, three hydrogens (the B5 terminal hydrogen and 2 bridging hydrogens) move to *endo*-positions on B5, B6, and B7 to form INT1. In INT1, the decreased B–O bond length (1.61 Å) is accompanied by a corresponding increase in the B5–B6 distance from 1.81 to 2.40 Å, but at this point, there is no additional lengthening of the B–Cl bond. As the oxygen moves closer (1.49 Å) to B6 to form TS2, the chlorine begins to detach

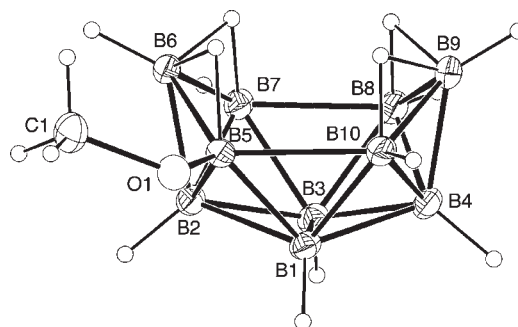


**Figure 3.** ORTEP drawings of the crystallographically determined structures of 5OMe. Selected bond distances (Å) and angles (°): B5–O1, 1.370(3); O1–C1, 1.434(2); B5–B6, 1.826(3); B6–B7, 1.803(3); B5–B10, 2.046(3); B8–B7, 1.968(3); B5–B1, 1.761(3); B1–B10, 1.746(3); B8–B3, 1.757(3); B6–B2, 1.732(3); B2–B3, 1.780(3); B4–B9, 1.718(3); B7–B3, 1.756(2); C1–O1–B5, 120.82(15); B6–B5–B10, 112.99(14); O1–B5–B2, 131.29(15); O1–B5–B1, 121.56(15); B5–B10–B9, 117.61(13); B5–B1–B10, 71.38(11); B7–B3–B8, 68.14(11); B5–B6–B7, 104.90(13); B8–B9–B10, 105.79(14).

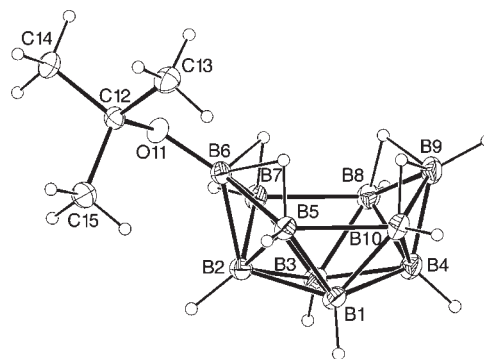


**Figure 4.** ORTEP drawing of the crystallographically determined structure of 6-((CH<sub>3</sub>)<sub>3</sub>CO)-B<sub>10</sub>H<sub>13</sub>. Selected bond distances (Å) and angles (°): (a) B6–O11, 1.335(2); O11–C12, 1.470(2); B6–B5, 1.826(3); B5–B10, 1.994(3); B5–B1, 1.764(3); B5–B2, 1.806(3); B6–B2, 1.739(3); B9–B10, 1.793(3); B9–B4, 1.718(3); C12–O11–B6, 129.10(15); O11–B6–B5, 133.69(17); O11–B6–B7, 122.91(16); B6–B5–B10, 118.50(15); O11–B6–B2, 136.39(16); B5–B10–B9, 118.03(15); B5–B6–B7, 103.07(14); B10–B9–B8, 104.63(15).

(B6–Cl, 2.42 Å) from the cage forming a five-membered B–Cl–H–O–B ring structure (Figure 8) that allows the Cl to bond with the methanolic hydrogen (1.74 Å). In the final step, the hydrogen is transferred from the oxygen to the chlorine (H–Cl, 1.32 Å) with the elongated H–O bond length (1.82 Å) typical of those found for hydrogen-bonded ethers.<sup>30</sup> As a result of the chlorine leaving the cage, the *endo*-B6–H moves to the vacated terminal B6 position and the *endo*-hydrogens on B5 and B7 move into bridging positions. The hydrogen-bonded HCl/decaboranyl–ether adduct is not stable under the experimental reaction conditions, since the HCl is immediately neutralized by NaHCO<sub>3</sub> to liberate the final decaboranyl ether.

An analogous pathway was found for the reaction of methanol with 5Cl (Figure 9). Nucleophilic attack of the alcohol at B6 occurs through TS3 to form INT2. The INT2 structure is similar to INT1, with a 1.61 Å B6–O distance and three *endo*-hydrogens. As the oxygen moves closer (1.49 Å), the TS4 transition state is formed, which, like TS2, has a cyclic five-membered configuration

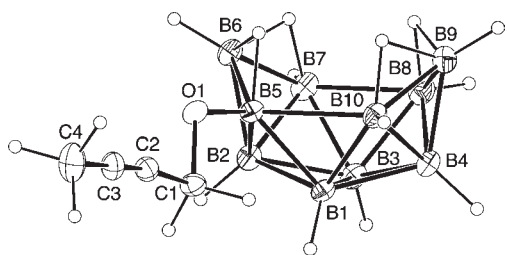


**Figure 5.** ORTEP drawing of the crystallographically determined structure of one of the two independent molecules of 5-(CH<sub>3</sub>C≡CCH<sub>2</sub>O)-B<sub>10</sub>H<sub>13</sub>. Selected bond distances (Å) and angles (°): B5–O1, 1.3828(17); O1–C1, 1.4336(15); B5–B6, 1.793(2); B5–B10, 2.044(2); B8–B7, 1.954(2); B6–B7, 1.792(2); B5–B1, 1.7605(19); B1–B10, 1.747(2); B6–B2, 1.726(2); B4–B9, 1.720(2); B7–B3, 1.743(2); C1–O1–B5, 117.61(10); B6–B5–B10, 114.93(10); O1–B5–B2, 131.45(11); O1–B5–B1, 126.77(10); B5–B10–B9, 116.61(10); B5–B1–B10, 71.28(8); B7–B3–B8, 67.91(9); B5–B6–B7, 105.31(10); B8–B9–B10, 105.45(11).

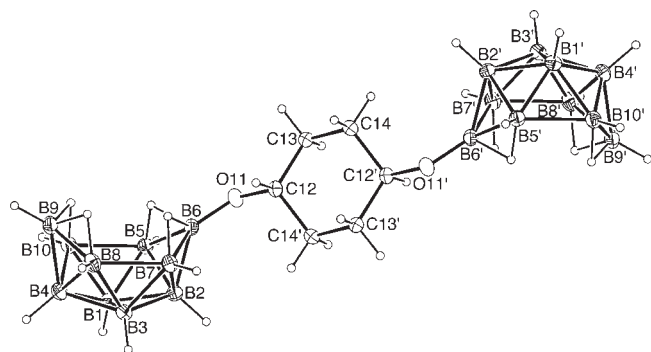


**Figure 6.** ORTEP drawing of the crystallographically determined structure of 6,6'-(OC<sub>6</sub>H<sub>10</sub>O)-(B<sub>10</sub>H<sub>13</sub>)<sub>2</sub>. Selected bond distances (Å) and angles (°): B6–O11, 1.3549(19); O11–C12, 1.4506(17); B6–B5, 1.804(2); B5–B10, 1.980(2); B5–B1, 1.749(2); B1–B10, 1.748(2); B5–B2, 1.799(2); B6–B2, 1.733(2); B9–B4, 1.717(3); C12–O11–B6, 122.22(12); O11–B6–B5, 123.37(13); B6–B5–B10, 118.00(12); B5–B6–B7, 104.11(11); B8–B9–B10, 104.73(12).

**Table 4.** Crystallographically Determined B–O Bonds Lengths and Angles

	B–O length (Å)	C–O–B angle (°)
B(OCH <sub>3</sub> ) <sub>3</sub> <sup>24</sup>	1.359(6)	119.7
[B(OCH <sub>3</sub> ) <sub>4</sub> ] <sup>−25</sup>	1.46 (avg)	116 (avg)
6-(ClC <sub>2</sub> H <sub>4</sub> OC <sub>2</sub> H <sub>4</sub> O)-B <sub>10</sub> H <sub>13</sub>	1.3548(13)	120.74(8)
5-(ClC <sub>2</sub> H <sub>4</sub> OC <sub>2</sub> H <sub>4</sub> O)-B <sub>10</sub> H <sub>13</sub>	1.3604(19)	122.93(11)
5-(CH <sub>3</sub> O)-B <sub>10</sub> H <sub>13</sub> ( <b>SOMe</b> )	1.370(3)	120.82(15)
6-((CH <sub>3</sub> ) <sub>3</sub> CO)-B <sub>10</sub> H <sub>13</sub>	1.335(2)	129.10(15)
5-(CH <sub>3</sub> C≡CCH <sub>2</sub> O)-B <sub>10</sub> H <sub>13</sub>	1.3828(17)	117.61(10)
6,6'-(OC <sub>6</sub> H <sub>10</sub> O)-(B <sub>10</sub> H <sub>13</sub> ) <sub>2</sub>	1.3549(19)	122.22(12)
2-(CH <sub>3</sub> O)-1,12-C <sub>2</sub> B <sub>10</sub> H <sub>11</sub> <sup>5</sup>	1.3884(16)	119.76(10)
[(C <sub>2</sub> H <sub>5</sub> O)-B <sub>12</sub> H <sub>11</sub> <sup>2-</sup> ] <sup>26</sup>	1.442(5)	115.9(3)
[2-(ClC <sub>4</sub> H <sub>8</sub> O)-1-CB <sub>11</sub> H <sub>11</sub> <sup>−</sup> ] <sup>27</sup>	1.409(3)	118.4(2)

with an elongated B6–Cl (2.55 Å) distance (Figure 10) that facilitates the initial H–Cl bonding interaction (H–Cl, 1.73 Å). In the final step, the hydrogen transfer from the oxygen (H–O,

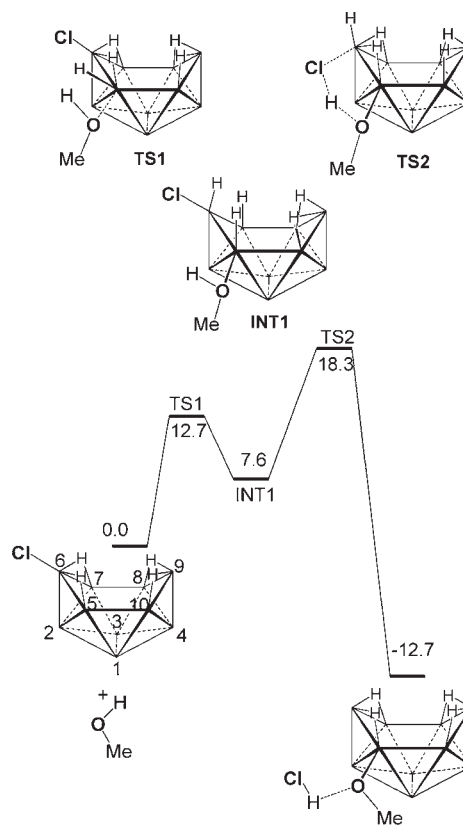


**Figure 7.** DFT calculated pathway from **6Cl** to **SOMe**. Calculations performed at the B3LYP/6-311G(d) level of theory at 298 K. Electronic energies are given in kcal/mol.

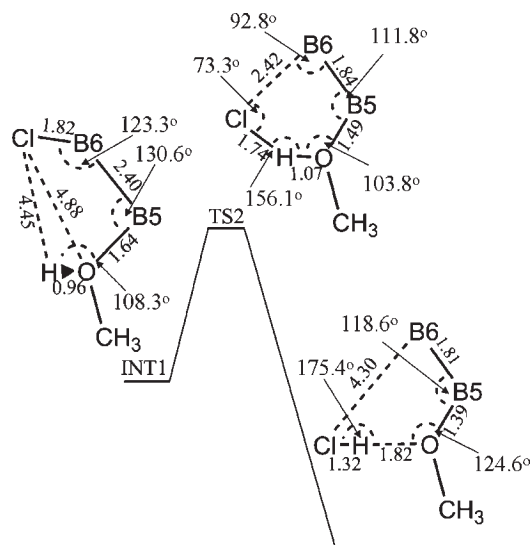


**Figure 8.** Bond distances and angles in the 5-membered ring portion of INT1, TS2, and the hydrogen-bonded combination of **6OMe** and HCl.

1.87 Å) to the chlorine (H–Cl, 1.31 Å) is complete to again produce the hydrogen-bonded decaboranyl ether. The chlorine is no longer attached to the cage and the *endo*-B5-H has moved to the vacated terminal B5-position with the *endo*-hydrogens on B5 and B7 moving back into bridging positions. Again, under the



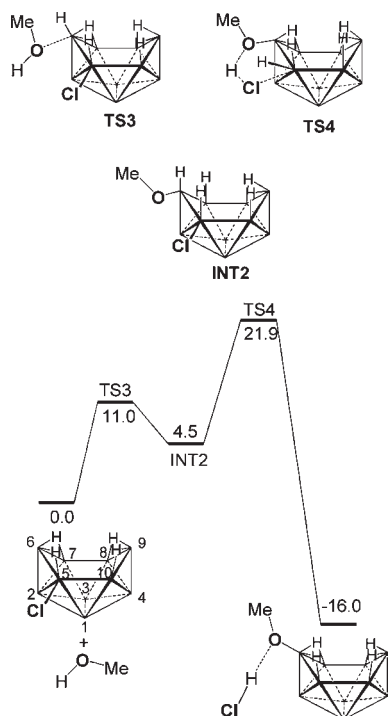


**Figure 9.** DFT calculated pathway from **5Cl** to **6OMe**. Calculations performed at the B3LYP/6-311G(d) level of theory at 298 K. Electronic energies are given in kcal/mol.

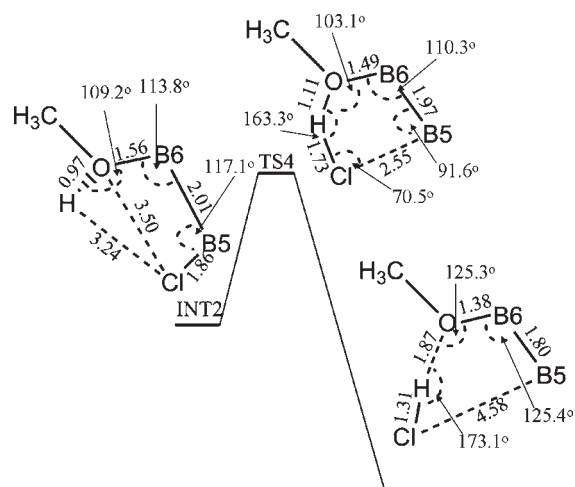


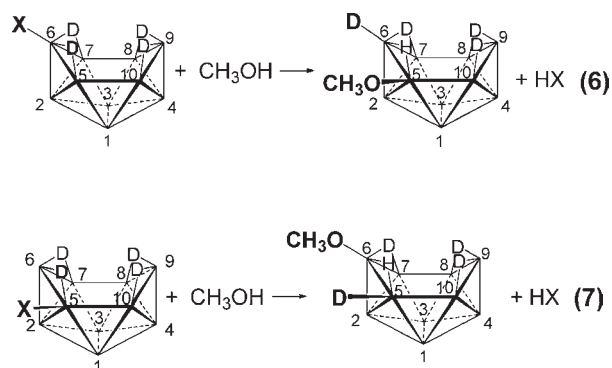
**Figure 10.** Bond distances and angles in the 5-membered ring portion of **INT2**, **TS4**, and the hydrogen-bonded combination of **6OMe** and **HCl**.

experimental reaction conditions, the hydrogen-bonded **HCl** is neutralized by  $\text{NaHCO}_3$  to liberate **6OMe**.

The higher activation energy of **TS4** (21.9 kcal/mol) compared to that of **TS2** (18.3 kcal/mol) is consistent with the slower rates of the **5X** reactions compared to those of **6X**. Likewise, optimization of **TS2** for the other 6-halodecaboranes found that the activation energy decreased in order **6F** (26.5 kcal/mol) > **6Cl** > **6Br** (13.4 kcal/mol) > **6I** (11.9 kcal/mol) consistent with the observed reaction rates (**6I**, **6Br** > **6Cl**  $\gg$  **6F**). Despite the relatively fast rates of the reactions of alcohols with **6I**, the ease of the isomerization of **6I** to **5I** under slightly basic conditions<sup>2</sup> resulted in final products of lower purity than those formed from **6Br**.

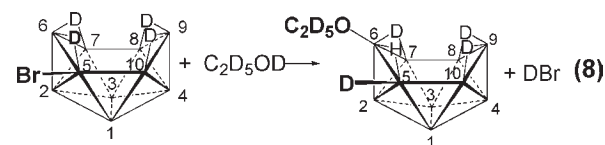
**Deuterium Labeling Studies.** Complete bridge deuteration without deuterium incorporation into any terminal B–H positions had been previously achieved for  $\text{B}_{10}\text{H}_{14}$  by its reaction with a biphasic mixture of  $\text{D}_2\text{O}$  and dioxane at room temperature and short reaction times.<sup>31</sup> Likewise, when **6Br** or **5Br** were stirred in biphasic  $\text{CDCl}_3/\text{D}_2\text{O}$  mixtures, analysis by  $^1\text{H}$  and  $^{11}\text{B}$  NMR (Figures S1 and S2, Supporting Information) showed selective deuterium exchange of all four bridging hydrogens with no measurable deuterium incorporation at any terminal B–H sites.<sup>32</sup>

According to the mechanisms in Figures 7 and 9, the reactions of the bridge-deuterated halodecaboranes with methanol should result in one of the bridging deuterons moving to the position vacated by the halogen (i.e., the bold **D** in eqs 6 and 7).



As predicted by the proposed mechanism, a comparison of the  $^{11}\text{B}$  NMR spectrum of **5OMe**, a product of the reaction of **6Br** with methanol (according to eq 1), to that of the product of the reaction of  $\mu\text{-D}_4\text{-6Br}$  with either  $\text{CH}_3\text{OH}$  (eq 6, X = Br) or  $\text{CD}_3\text{OD}$  showed that the doublet B6 resonance in the **5OMe** spectrum (Figure 11a) had changed to a singlet in the Figure 11b,c spectra indicating deuterium incorporation at the B6 terminal position.<sup>33</sup> The peak is sharper when  $\text{CH}_3\text{OH}$  is replaced with  $\text{CD}_3\text{OD}$  since the absence of a methanolic hydrogen eliminates any presubstitution H/D exchange with the bridging deuterons that would then result in some hydrogen incorporation at B6.

When  $\mu\text{-D}_4\text{-5Br}$  was reacted with  $\text{C}_2\text{D}_5\text{OD}$  in  $\text{CDCl}_3$  (eq 8) at 70 °C, the  $^{11}\text{B}$  NMR spectrum of the  $\mu\text{-D}_3\text{-5-D-6-(C}_2\text{D}_5\text{O)-B}_{10}\text{H}_9$  product showed a broadened resonance at  $\sim -15.5$  ppm (B5,7, as assigned in Figure S2, Supporting Information) consistent with the superposition of a singlet and doublet (B5 and B7, respectively, in eq 8) indicative of incorporation of deuterium into one of these vertices (Figure 12).<sup>34</sup> This observation is again consistent with the mechanism shown in Figure 9.



In summary, combined experimental and computational studies indicate that the reactivity imparted by the halo-substituents of the 5- and 6-halodecaboranes activates nucleophilic attack by the alcohol at an adjacent boron site, ultimately substituting alkoxide for halide. The unusual regioselectivity observed for these substitution reactions resembles that of an organic  $\text{S}_{\text{N}}2'$  reaction (eq 9), since, unlike in conventional  $\text{S}_{\text{N}}1$  and  $\text{S}_{\text{N}}2$  substitution reactions where the incoming group takes the place

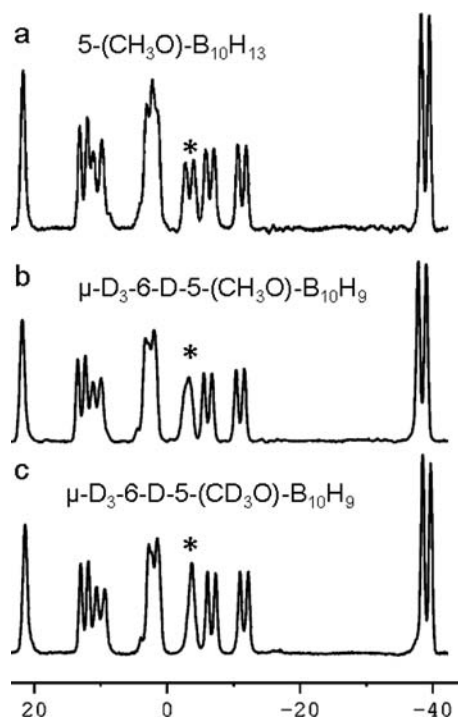


**Figure 11.**  $^{11}\text{B}$  NMR spectrum of the products of the following reactions: (a)  $6\text{Br} + \text{CH}_3\text{OH}$ , (b)  $\mu\text{-D}_3\text{-}6\text{-D-}5\text{-}(\text{CH}_3\text{O})\text{-B}_{10}\text{H}_9$ , and (c)  $\mu\text{-D}_3\text{-}6\text{-D-}5\text{-}(\text{CD}_3\text{O})\text{-B}_{10}\text{H}_9$ . The \* denotes the B6 resonance.

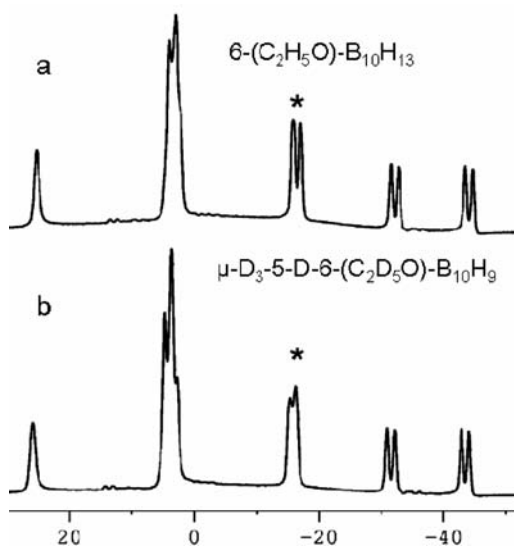
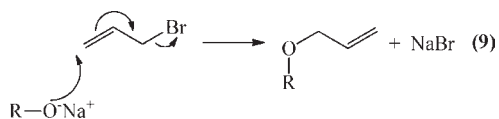


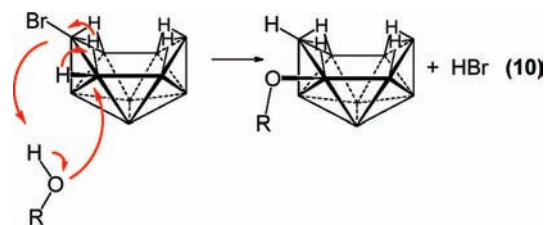
**Figure 12.**  $^{11}\text{B}$  NMR spectrum of the products of the following reactions: (a)  $5\text{Br} + \text{C}_2\text{H}_5\text{OH}$  and (b)  $\mu\text{-D}_3\text{-}5\text{-D-}6\text{-}(\text{C}_2\text{D}_5\text{O})\text{-B}_{10}\text{H}_9$ . The \* denotes the B5,7 coincident resonance.

of the leaving group, the substitution occurs at a site away from the leaving group.



In the organic  $\text{S}_{\text{N}}2'$  reactions, electrons are moved through the  $\pi$ -system to the leaving group, while in the halodecaborane

substitution reactions, hydrogen-migration provides the pathway for electron transport (eq 10).



These reactions now provide general synthetic routes to decaboranyl ethers starting with the readily available 6- and 5-halodecaboranes. A range of 1°, 2°, and 3° ethers have been produced bearing polymerizable groups (alkenes, alkynes), nucleophiles (thiol), and electrophiles (alkyl halides, succinimide), as well as new types of polyol-derived linked-cage compounds. The results of our ongoing investigations of the chemical properties and applications of these new decaboranyl ethers will be reported in future publications.

## ■ ASSOCIATED CONTENT

**S Supporting Information.** Full experimental and spectroscopic details for all synthesized compounds and DFT optimized Cartesian-coordinates and energies for relevant compounds and reaction steps. This material is available free of charge via the Internet at <http://pubs.acs.org>.

## ■ AUTHOR INFORMATION

### Corresponding Author

\*E-mail: [lsneddon@sas.upenn.edu](mailto:lsneddon@sas.upenn.edu).

## ■ ACKNOWLEDGMENT

We gratefully acknowledge the National Science Foundation and US Department of Energy for the support of this research.

## ■ REFERENCES

- (1) Ewing, W. C.; Carroll, P. J.; Sneddon, L. G. *Inorg. Chem.* **2008**, *47*, 8580–8582.
- (2) Ewing, W. C.; Carroll, P. J.; Sneddon, L. G. *Inorg. Chem.* **2010**, *49*, 1983–1994.
- (3) Sivaev, I. B.; Bregadze, V. I.; Sjöberg, S. *Collect. Czech. Chem. Commun.* **2002**, *67*, 679–727 and references therein.
- (4) Sivaev, I. B.; Prikaznov, A. V.; Naoufal, D. *Collect. Czech. Chem. Commun.* **2010**, *75*, 1149–1199.
- (5) Kabytaev, K. Z.; Mukhin, S. N.; Glukhov, I. V.; Starikova, Z. A.; Bregadze, V. I.; Beletskaya, I. P. *Organometallics* **2009**, *28*, 4758–4763.
- (6) (a) Nie, Y.; Hu, C.-H.; Li, X.; Yong, W.; Dou, J.-M.; Sun, J.; Jin, R.-S.; Zheng, P.-J. *Acta Crystallogr.* **2001**, *C57*, 897–899. (b) Paxon, T. E.; Hawthorne, M. F. *Inorg. Chem.* **1975**, *14*, 1604–1607.
- (7) Hawthorne, M. F.; Miller, J. J. *J. Am. Chem. Soc.* **1960**, *82*, 500.
- (8) Loffredo, R. E.; Drullinger, L. F.; Slater, J. A.; Turner, C. A.; Norman, A. D. *Inorg. Chem.* **1976**, *15*, 478–480.
- (9) Stuchlík, J.; Heřmánek, S.; Plešek, J.; Stíbr, B. *Collect. Czech. Chem. Commun.* **1970**, *35*, 339–343.
- (10) Frisch, M. J.; Trucks, G. W.; Schlegel, H. B.; Scuseria, G. E.; Robb, M. A.; Cheeseman, J. R.; Montgomery, J. A., Jr.; Vreven, T.; Kudin, K. N.; Burant, J. C.; Millam, J. M.; Iyengar, S. S.; Tomasi, J.; Barone, V.; Mennucci, B.; Cossi, M.; Scalmani, G.; Rega, N.; Petersson, G. A.; Nakatsuji, H.; Hada, M.; Ehara, M.; Toyota, K.; Fukuda, R.; Hasegawa, J.; Ishida, M.; Nakajima, T.; Honda, Y.; Kitao, O.; Nakai, H.; Klene, M.; Li, X.; Knox, J. E.;

Hratchian, H. P.; Cross, J. B.; Adamo, C.; Jaramillo, J.; Gomperts, R.; Stratmann, R. E.; Yazyev, O.; Austin, A. J.; Cammi, R.; Pomelli, C.; Ochterski, J. W.; Ayala, P. Y.; Morokuma, K.; Voth, G. A.; Salvador, P.; Dannenberg, J. J.; Zakrzewski, V. G.; Dapprich, S.; Daniels, A. D.; Strain, M. C.; Farkas, O.; Malick, D. K.; Rabuck, A. D.; Raghavachari, K.; Foresman, J. B.; Ortiz, J. V.; Cui, Q.; Baboul, A. G.; Clifford, S.; Cioslowski, J.; Stefanov, B. B.; Liu, G.; Liashenko, A.; Piskorz, P.; Komaromi, I.; Martin, R. L.; Fox, D. J.; Keith, T.; Al-Laham, M. A.; Peng, C. Y.; Nanayakkara, A.; Challacombe, M.; Gill, P. M. W.; Johnson, B.; Chen, W.; Wong, M. W.; Gonzalez, C.; Pople, J. A. *Gaussian 03*, revision B.05; Gaussian, Inc.: Pittsburgh PA, 2003.

(11) SAINT version 7.68A: Bruker AXS Inc., Madison, WI, USA.

(12) SHELXTL version 6.14: Bruker AXS Inc., Madison, WI, USA.

(13) SADABS version 2008/1. Bruker AXS Inc., Madison, WI, USA.

(14) CrystalClear version 1.36: Rigaku Corporation Inc., The Woodlands, TX, USA.

(15) CrystalStructure: Crystal Structure Analysis Package. version 3.60. Rigaku Corporation Inc., The Woodlands, TX, USA.

(16) REQAB4: A Program for Absorption Correction of X-ray Diffraction Data, Jacobsen, R. A., Rigaku Corporation Inc., The Woodlands, TX, USA.

(17) Altomare, A.; Burla, M. C.; Camalli, M.; Cascarano, M.; Giacovazzo, C.; Guagliardi, A.; Moliterni, A.; Polidori, G. J.; Spagna, R. *J. Appl. Crystallogr.* **1999**, *32*, 115–119, SIR97.

(18) Sheldrick, G. M. *Acta Cryst.* **2008**, *A64*, 112–122.

(19) Beachell, H. C.; Schar, W. C. *J. Am. Chem. Soc.* **1958**, *80*, 2943–2945.

(20) Ingold, C. K. *Chem. Rev.* **1934**, *15*, 225–274.

(21) Finch, A.; Gardner, P. J.; Watts, G. B. *Trans. Faraday Soc.* **1967**, *63*, 1603–1607.

(22) Fenwick, J. T. F.; Wilson, W. J. *J. Chem. Soc. Dalton Trans.* **1972**, *13*, 1324–1326.

(23) (a) Barth, R. F. *Appl. Radiat. Isot.* **2009**, *67*, S3–S6. (b) Hatanaka, H.; Nakagawa, Y. *Int. J. Radiat. Oncol. Biol. Phys.* **1994**, *28*, 1061–1066.

(24) (a) Sivaev, I. B.; Bregadze, V. I. *Eur. J. Inorg. Chem.* **2009**, 1433–1450 and references therein. (b) Ma, L.; Hamdi, J.; Wong, F.; Hawthorne, M. F. *Inorg. Chem.* **2006**, *45*, 278–285.

(25) (a) Li, Y.; Sneddon, L. G. *J. Am. Chem. Soc.* **2008**, *130*, 11494–11502. (b) Roth, M.; Meyer, F.; Paetzold, P. *Collect. Czech. Chem. Commun.* **1997**, *62*, 1299–1309. (c) Paetzold, P. *Eur. J. Inorg. Chem.* **1998**, 143–153. (d) Garrett, P. M.; Ditta, G. S.; Hawthorne, M. F. *J. Am. Chem. Soc.* **1971**, *93*, 1265–1266.

(26) Hartl, M. A.; Williams, D. J.; Acatrinei, A. I.; Stowe, A.; Daemen, L. L. Z. *Anorg. Allg. Chem.* **2007**, *633*, 120–126.

(27) Alcock, M. W.; Hagger, R. M.; Harrison, W. D.; Wallbridge, M. G. H. *Acta Crystallogr.* **1982**, *B38*, 676–677.

(28) Peymann, T.; Lork, E.; Gabel, D. *Inorg. Chem.* **1996**, *35*, 1355–1360.

(29) Mair, F. S.; Morris, J. H.; Gaines, D. F.; Powell, D. *J. Chem. Soc., Dalton Trans.* **1993**, 135–141.

(30) (a) Legon, A. C. *Faraday Discuss.* **1994**, *97*, 19–33. (b) Ferreira, F. C.; Oliveira, B. G.; Ventura, E.; do Monte, S. A.; Braga, C. F.; Araújo, R. C. M. U.; Ramos, M. N. *Spectrochim. Acta A* **2006**, *64*, 156–160. (c) Antolínez, S.; López, J. C.; Alonso, J. L. *Chem. Phys. Lett.* **2001**, *334*, 250–256.

(31) Hawthorne, M. F.; Miller, J. J. *J. Am. Chem. Soc.* **1958**, *80*, 754.

(32) While the parent compound B<sub>10</sub>H<sub>14</sub> was not found to undergo H/D exchange when stirred in mixtures of D<sub>2</sub>O and nonethereal solvents (ref 31), **6Br** quickly underwent bridge-deuteration with D<sub>2</sub>O in CDCl<sub>3</sub>. This is likely an indication of the enhanced acidity of the halogenated cages relative to B<sub>10</sub>H<sub>14</sub>.

(33) Since <sup>11</sup>B-D coupling is small, evidence for terminal deuteration would be found in the collapse of B-H coupling normally seen in the <sup>11</sup>B NMR spectra of each decaboranyliether. For example, for BD<sub>4</sub><sup>-</sup>: J<sub>B-D</sub> = ~12 Hz, compared to BH<sub>4</sub><sup>-</sup>: J<sub>B-H</sub> = ~80 Hz. See: Than, C.; Morimoto, H.; Andres, H.; Williams, P. G. *J. Labeled Compd. Radio. Pharm.* **1998**, *38*, 693–711.

(34) Owing to the increased rate of deuterium exchange between bridging deuterium and ethanolic hydrogen at elevated temperatures, the reactions  $\mu\text{-D}_4\text{-5Br}$  with CH<sub>3</sub>OH resulted in products with a mix of H/D incorporation at B6.